Biosensors and Bioelectronics 142 (2019) 111497

Contents lists available at ScienceDirect

Biosensors and Bioelectronics

journal homepage: www.elsevier.com/locate/bios

A novel triarylboron based ratiometric fluorescent probe for in vivo targeting and specific imaging of cancer cells expressing abnormal concentration of GGT

Jun Liu[a,*,1], Shilu Zhang[a,1], Bin Zhao[b], Chengyi Shen[a], Xiaoming Zhang[c,**], Guoqiang Yang[b,***]

[a] Sichuan Key Laboratory of Medical Imaging, Affiliated Hospital of North Sichuan Medical College & Department of Chemistry, School of Preclinical Medicine, North Sichuan Medical College, Nanchong, 637000, China
[b] Key Laboratory of Photochemistry, Institute of Chemistry, University of Chinese Academy of Sciences, Chinese Academy of Sciences, Beijing, 100190, China
[c] Department of Radiology, Affiliated Hospital of North Sichuan Medical College, China

ARTICLE INFO

Keywords:
Fluorescence
Triarylboron
GGT
Ovarian cancers
Targeting

ABSTRACT

Abnormal expression of γ-glutamyltranspeptidase (GGT) in living organisms is closely associated with tumorigenesis. However, few reported fluorescence probes can specifically respond to abnormal concentration of GGT. Here, by functionalizing triarylboron moiety with three GGT-specific substrate (GSH) units, a novel fluorescence probe, TAB-3-GSH, was developed for detecting GGT. The results showed that TAB-3-GSH selectively responds to abnormally high levels of GGT (100–1000 U/L) rather than to normal GGT levels (< 100 U/L) with ratiometric readout, since the amide linkage can be further hydrolyzed under high GGT levels. TAB-3-GSH was also capable of differentiating GGT-overexpressing ovarian cancer cells from normal cells, because of an improvement in the probe's cell membrane permeability upon reaction with GGT. Moreover, the probe could achieve selective imaging of SKOV-3 tumor site in xenograft mice model. Thus, TAB-3-GSH is a promising probe for tumor targeting in vivo.

1. Introduction

Cancer is one of the deadliest diseases worldwide, and has become a serious threat to human health(Siegel et al., 2018). One of the main challenges in cancer treatment is the timely and accurate diagnosis of cancer at an early stage, which is very important for the prevention and mitigation of cancer progression(Greenlee et al., 2000). Some tumor-related biomarkers can provide effective diagnosis information and prognosis indications of certain cancers (Blum et al., 2007; Bremer et al., 2001; Wu and Qu, 2015). Typically, γ-glutamyltranspeptidase (GGT), a cell membrane-bound enzyme that selectively catalyzes the cleavage of the γ-glutamyl bond in GSH, is overexpressed in cells of a variety of human cancers, such as cervical and ovarian cancers (Hanigan et al., 1994; Yao et al., 2000). It has been reported that GGT promotes tumor progression, invasion and anticancer-drug resistance, and a high level of GGT in serum is closely related to an increased risk of cancer (Pompella et al., 2006; Hu et al., 2012; Fraser et al., 2007; Ozcan et al., 2012). Therefore, GGT is considered to be a biomarker for cancer detection and has been used as a diagnostic and prognostic index of gynecologic cancers in clinical trials (Grimm et al., 2013; Ostapenko et al., 2011; Vandenhaute et al., 2011).

Fluorescence probes are a promising and powerful tool for tumor-related biomarker imaging because of its high specificity, sensitivity, and non-toxicity in live cells or tissues (Wolfbeis, 2015). Based on the GGT-catalyzed cleavage of γ-glutamyl bond, researchers have successfully designed and synthesized several fluorescence probes for GGT (Hou et al., 2014; Li et al., 2015; Tong et al., 2016; Wang et al., 2015). Most of them, including our previously reported bioluminescent probe (Berk and Korenblat, 2011), have attempted to achieve higher sensitivity and lower detection limits. However, we noticed that the normal GGT level in blood is 5–55 U/L for adult females and 15–85 U/L for adult males, which exceeds the maximum detection concentration of most reported GGT fluorescent probes (Li et al., 2017a). In other words, these probes can be fully reacted to produce maximum fluorescence response for GGT even when they enter the normal body, and thus demonstrate no specificity to cancer patients, whose GGT levels can

* Corresponding author.
** Corresponding author.
*** Corresponding author.
E-mail addresses: ustbliujun@iccas.ac.cn (J. Liu), zhangxm@nsmc.edu.cn (X. Zhang), gqyang@iccas.ac.cn (G. Yang).
[1] Authors contributed equally.

https://doi.org/10.1016/j.bios.2019.111497
Received 5 May 2019; Received in revised form 5 July 2019; Accepted 8 July 2019
Available online 10 July 2019

reach hundreds of units per liter (Gowda et al., 2009). Therefore, a potential probe for in vivo cancer targeted imaging should specially respond to abnormal GGT concentration rather than normal GGT concentration. Moreover, an ideal fluorescence probe should provide ratiometric readout and a large two-photon (TP) cross section to minimize some interfering factors and overcome the shortcomings of single photon excitation, respectively (Park et al., 2016; Li et al., 2017b; Bae et al., 2013; Zhou et al., 2014).

As a new research direction, π-conjugated triarylboron compounds have aroused much interest because of their unique structure and excellent photophysical properties (Jäkle, 2010; Wade et al., 2010; Ji et al., 2017). The three aromatic groups in their molecular structure can be easily modified at multiple sites to achieve diverse functions. Based on this, we have previously developed a series of triarylboron-based biological fluorescent probes, including for imaging intracellular temperature, hydrogen sulfide, and RNA (Liu et al., 2015, 2016, 2017; Li et al., 2014; Urano et al., 2011). These studies showed that triarylboron compounds possess many favorable fluorescence features, including high quantum yields, large TP absorption cross sections, and extreme sensitivity to microenvironmental changes for ratiometric readout. Therefore, theoretically, it is also possible to develop GGT fluorescent probes with excellent properties by reasonably designing and functionalizing the triarylboron compounds.

Thus, in this study, we aimed to develop novel fluorescent probes for detecting abnormal concentration of GGT. In order to achieve this we functionalized a triarylboron center with three GSH groups by using amide bond linkage to synthesize TAB-3-GSH based on the following initial considerations: (1) the three surrounding GSH groups will be hydrolyzed in the presence of GGT, which may result in an obvious change in the fluorescence of the sensitive central triarylboron; (2) the multiple GSH groups can increase the demand for GGT concentration and thus achieve the required response to abnormal concentration GGT; (3) the six strong hydrophilic carboxylic groups in its molecular structure will result in poor cell membrane permeability, which will be improved after the carboxyl groups are made unavailable due to reaction with GGT, thus achieving selective imaging of cells showing high GGT expression. Interestingly, in further experiments, we found that high concentration of GGT could further catalyze the hydrolysis of amide linkage, resulting in greater fluorescence changes and providing a ratiometric readout, which may be used as a new strategy for designing fluorescence probes for abnormal concentration GGT. Three other reference compounds, TAB-3-Cys-Gly, TAB-3-Cys, and TAB-3-GSH-Et, were also synthesized for a comparative study (Scheme 1). The results showed that TAB-3-GSH exhibits greater ratiometric fluorescence responsiveness and better cell selectivity than these reference compounds. The subsequent cell imaging experiments also verified that TAB-3-GSH is capable of specific, rapid, and accurate differentiation of GGT-overexpressing cancer cells, such as those of ovarian cancer, from normal cells. Moreover, TAB-3-GSH showed a high selectively for the real-time and non-invasive targeted imaging of ovarian cancer sites in mouse tumor models.

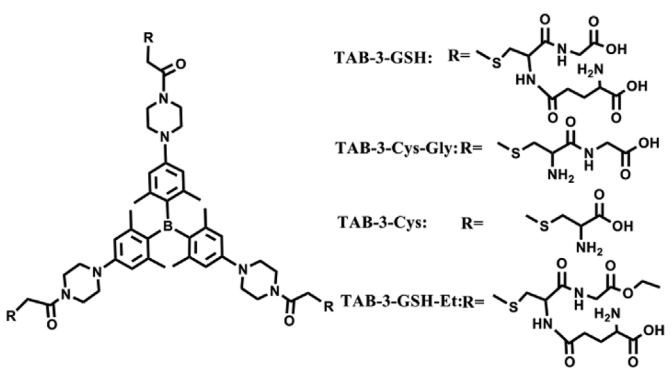

Scheme 1. Chemical structure of TAB-3-GSH, TAB-3-Cys-Gly, TAB-3-Cys and TAB-3-GSH-Et.

2. Experimental

2.1. General information

General chemical reagents were purchased from Beijing InnoChem Science & Technology Co (Beijing, China) and used without further purification. GGT were obtained from Sigma-Aldrich. Absorption spectra were recorded on Hitachi UV-3010 (Hitachi, Tokyo, Japan). The fluorescence spectra were obtained on Hitachi F-7000 (Hitachi, Tokyo, Japan). Cells were analyzed using a confocal microscope (OLYMPUS FV 1000-IX81 Olympus Corporation, Tokyo, Japan). NIH/3T3 cells were obtained from KaijiBio TECH Co. Ltd. HUVEC-1 and SKOV-3 cells were obtained from Cell Bank of Chinese Academy of Sciences. ^{1}H NMR spectra were obtained on BrukerAvance III 400 H (400 MHz) spectrometers (Bruker, Karlsruhe, Germany). In vivo small animal imaging system (In-Vivo MS FX PRO, Bruker, Germany).

2.2. Synthesis

The synthesis of TAB-3-GSH, TAB-3-Cys-Gly, TAB-3-Cys, and TAB-3-GSH-Et are shown in supporting information (Scheme S1).

2.3. Cell culture and imaging

Human umbilical vein endothelial cells (HUVEC-1) were cultured in Bronchial Epithelial Cell Growth Medium supplemented with 10% fetal bovine serum (FBS). Human ovarian cancer cells (SKOV-3) and Mouse fibroblast cells (NIH/3T3) were cultured in Dulbecco's Modified Eagle Medium (DMEM) with glucose (4.5 g/L), L-glutamine, sodium pyruvate, and 10% fetal bovine serum (FBS). The cells were plated on glass bottomed dishes at 37 ˚C under 5% CO2 atmosphere before imaging. Cell imaging were conducted using a confocal microscope FV1000-IX81 and were analyzed with FV10-ASW software.

Cells, pre-washed twice, were incubated with 10 μM of probes in cultured medium without FBS at 37 ˚C under 5% CO2 for 15min. Then the cells were washed with PBS to remove unbounded probes for six times before in situ imaging by Olympus FV1000-IX81 confocal laser scanning microscopy using oil objective, with excitation by 405 nm.

2.4. Tumor model and in vivo imaging

Nude mice 6–7 weeks old were provided by the Laboratory Animal Center of North Sichuan Medical College, Nanchong, China. All procedures involving animals were performed according to a protocol approved by the Institutional Animal Care and Treatment Committee of North Sichuan Medical College. These nude mice were subcutaneously injected with 1 × 106 SKOV-3 cells in the right rear thigh under aseptic conditions. Then they were individually housed under specific pathogen-free conditions with free access to food and water until the formed tumor grow to approximately 0.5 cm in diameter by measuring caliper; tumor growth to this size took about a month. These tumor-bearing mice were fasting for 24 h and then were anesthetized by intraperitoneal injection of 0.05 mL 3% aqueous solution of pentobarbital. The mice were then placed into the small animal imager and injected intraperitoneally with a certain amount of probe solution for imaging.

3. Results and discussion

3.1. Fluoresent response for GGT in vitro

We firstly measured the fluorescence spectra of TAB-3-GSH with the addition of different amounts GGT to test whether it can be used as a

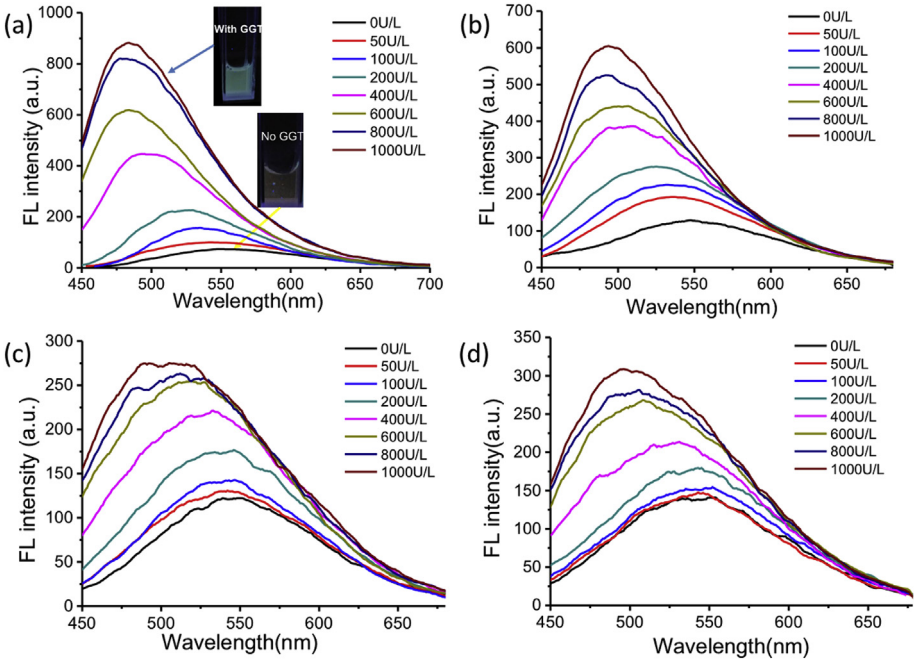

Fig. 1. Fluorescence spectra changes of (a) TAB-3-GSH, (b) TAB-3-Cys-Gly, (c)TAB-3-Cys and (d) TAB-3-GSH-Et (0.5 μM in 10 mM PBS) with the addition of different amounts of GGT at 37 °C for 15 min (λexc = 405 nm).

fluorescent probe for GGT. Fig. 1a shows its fluorescence spectra, which demonstrated a slight change when GGT concentration was less than 100 U/L, which corresponds to the concentration range in normal human body. With increasing concentrations of GGT, the fluorescence intensity achieved by the probe at 480 nm increased and displayed a ~50-fold enhancement when the concentration of GGT reached 1000 U/L. In addition, maximum emission wavelength showed an obvious blue shift, providing a ratiometric readout, accompanied by visible fluorescence color change from weak yellow to intense green. The other three reference compounds, TAB-3-Cys-Gly, TAB-3-Cys, and TAB-3-GSH-Et, demonstrated similar fluorescence response tendency with TAB-3-GSH but a smaller magnitude of response in presence of GGT. Among them, TAB-3-Cys-Gly showed a 10-fold fluorescence enhancement, which was larger than that achieved with TAB-3-Cys and TAB-3-GSH-Et. This may imply that GGT can induce some reaction in the structure of TAB-3-Cys-Gly. Therefore, we further explored the recognition mechanism involved by utilizing high-resolution mass spectrometry to detect the reaction products.

The mixture of TAB-3-GSH and low concentration of GGT (100 U/L) demonstrated an obvious MALDI mass peak at 1233.55, indicating the producing of TAB-3-Cys-Gly (Fig. S3). The mixture of TAB-3-GSH and high concentration of GGT (1000 U/L) manifested an ESI mass peak at 237.09, exactly corresponding the product after the further hydrolysis of amide linkage in TAB-3-Cys-Gly structure (Fig. S4). The hydrolysis can also be confirmed by the presence of a series of MALDI mass peaks of related products after mixing TAB-3-Cys-Gly with high concentration of GGT (1000 U/L) (Fig. S5). Accordingly, we propose a mechanism that GGT catalyzes a two-step hydrolysis reaction of TAB-3-GSH as follows: (1) The γ-glutamyl bond of GSH group can be firstly hydrolyzed under low concentration of GGT to produce TAB-3-Cys-Gly; (2) The amide linkage of TAB-3-Cys-Gly may then be further hydrolyzed under higher concentration of GGT (Scheme 2). The proposed mechanism also can help us understand their different fluorescence response for GGT. TAB-3-GSH demonstrates greater fluorescence change than TAB-3-Cys-Gly after reacting with GGT because it undergoes a complete two-step hydrolysis process and TAB-3-Cys-Gly only happen the second hydrolysis reaction. The possible explanation for the less fluorescence response of TAB-3-GSH-Et and TAB-3-Cys for GGT can be attributed to their structural changes, which reduces their reactivity for the second hydrolysis reaction and make them cannot react completely in the hydrolysis process. The considerable TP cross section of TAB-3-Piperazine also makes it possible to conduct TP imaging (Fig. S6). The non-functionalized TAB-3-Piperazine, the fluorophore produced by hydrolysis, also exhibited a certain fluorescence blue shift and enhancement under high concentration of GGT, which may be attributed to its distribution into the low polar hydrophobic region of GGT's interior since its small molecular volume and amphiphilicity, which can also partially contribute to the fluorescence response of TAB-3-GSH for GGT (Fig. S7).

The ratio of fluorescence intensity of TAB-3-GSH at 480 nm and 550 nm also showed a ~11-fold change, making it easily to be ratioed and demonstrate a certain correlation with GGT levels (Fig. 2a and b). In addition, the reaction was complete in about 10 min, demonstrating a fast response speed (Fig. 2b). The selectivity of TAB-3-GSH for GGT was investigated by examining its fluorescence response for various potential coexisting species, including some common enzymes (trypsin, esterase, and apryrase), biologically relevant sulfur (glutathione, homocysteine, cysteine, and aminothiol), and nucleoside polyphosphate (RNA, ATP, ADP, and AMP). As depicted in Fig. 3d and Fig. S8, both TAB-3-GSH and TAB-3-Cys demonstrated high specificity for GGT over the other substances tested, indicating that both the first and second step of hydrolysis are selective for GGT.

3.2. GGT imaging in cellulo and in vivo

Based on the results of the in vitro experiments, we considered that TAB-3-GSH could be used effectively to distinguish cancer cells overexpressing GGT from normal cells. To further test this hypothesis, we firstly investigated the cell membrane permeability of TAB-3-GSH by incubating NIH/3T3 cells with the probe for 1 h and detected no fluorescence signal under confocal fluorescence microscope, indicating its poor cell membrane permeability resulting from the six strongly hydrophilic negatively charged carboxyl groups in its molecular structure (Fig. 3a). However, NIH/3T3 cells incubated with TAB-3-Cys-Gly and TAB-3-Piperazine, the hydrolysis product of TAB-3-GSH, for 30 min and 5 min, respectively, exhibited strong fluorescence, indicating

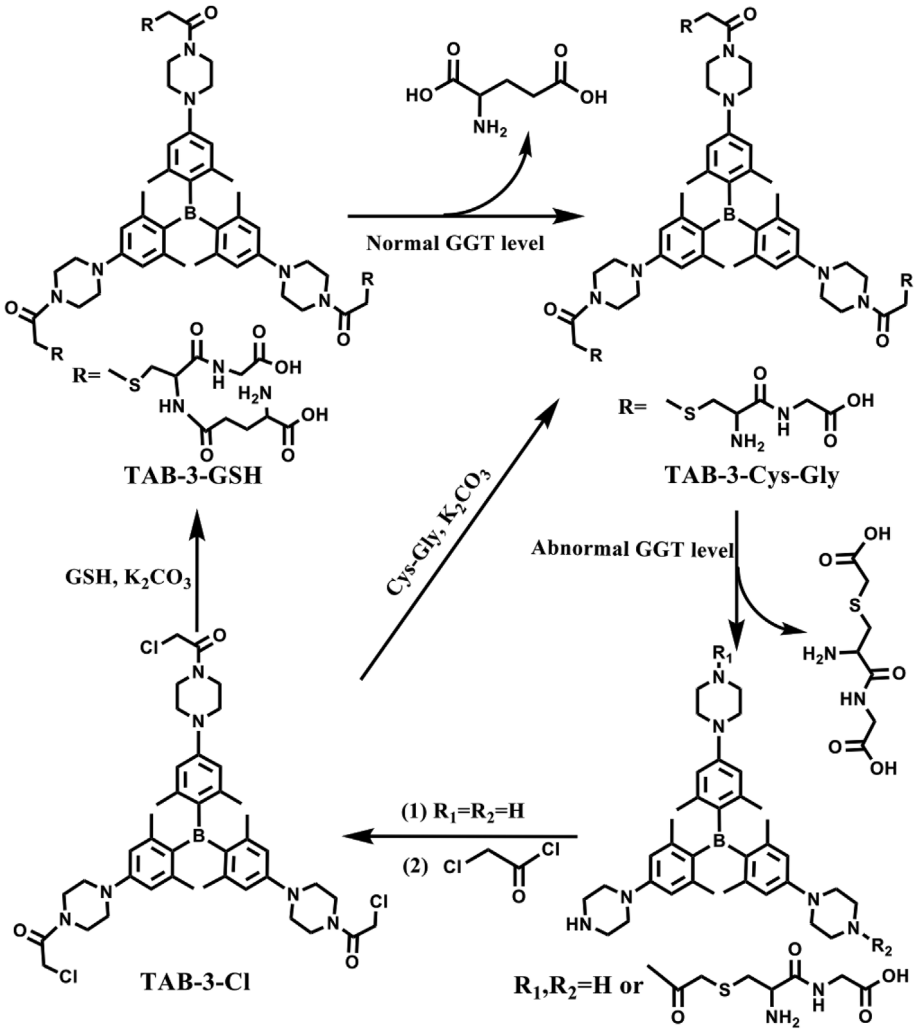

Scheme 2. Proposed reaction mechanism of TAB-3-GSH for GGT detection.

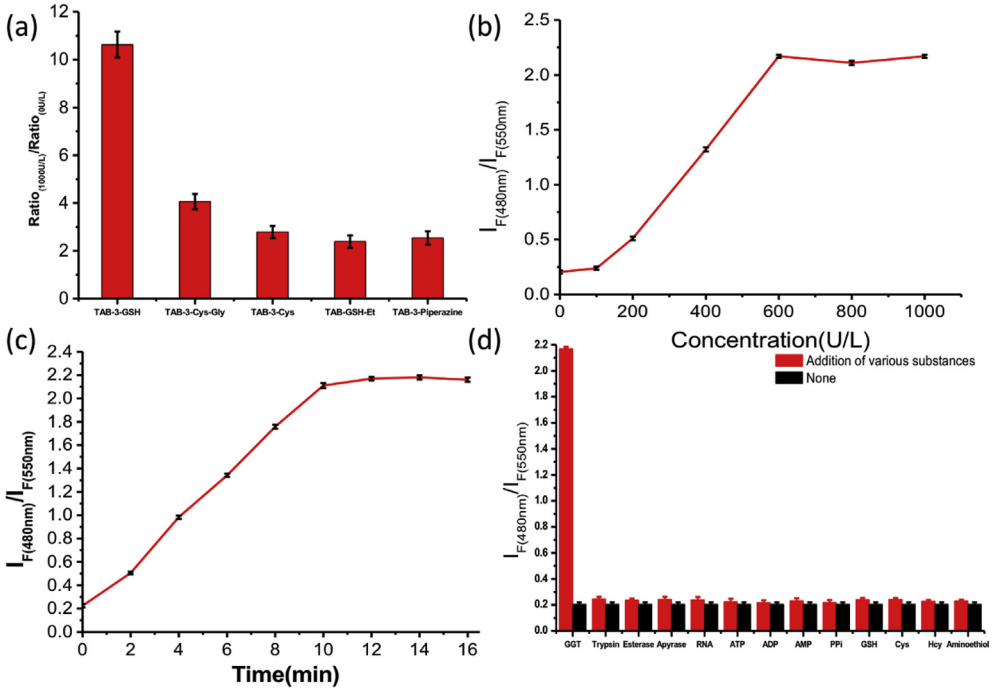

Fig. 2. (a) The change in the ratio of fluorescence intensity at 480 and 550 nm after and before reaction (CV = 1.8%, 2.1%, 1.3%, 1.5%, 2.1%). Correlation between the ratio (IF (480 nm)/IF(550 nm)) and (b) GGT concentrations (CV = 1.5%, 1.7%, 0.8%, 1.1%, 1.2%, 1.6%, 1.8%) and (c) reaction time (CV = 1.6%, 1.1%, 0.9%, 1.7%, 2.0%, 1.8%, 1.6%, 1.5%, 1.7%). (d) The ratio (IF (480 nm)/IF(550 nm)) of TAB-3-GSH after the addition of various substances (Addition of various substances: CV = 1.8%, 1.1%, 0.9%, 1.7%, 2.0%, 1.8%, 1.6%, 1.5%, 1.7%; None: CV = 1.5%).

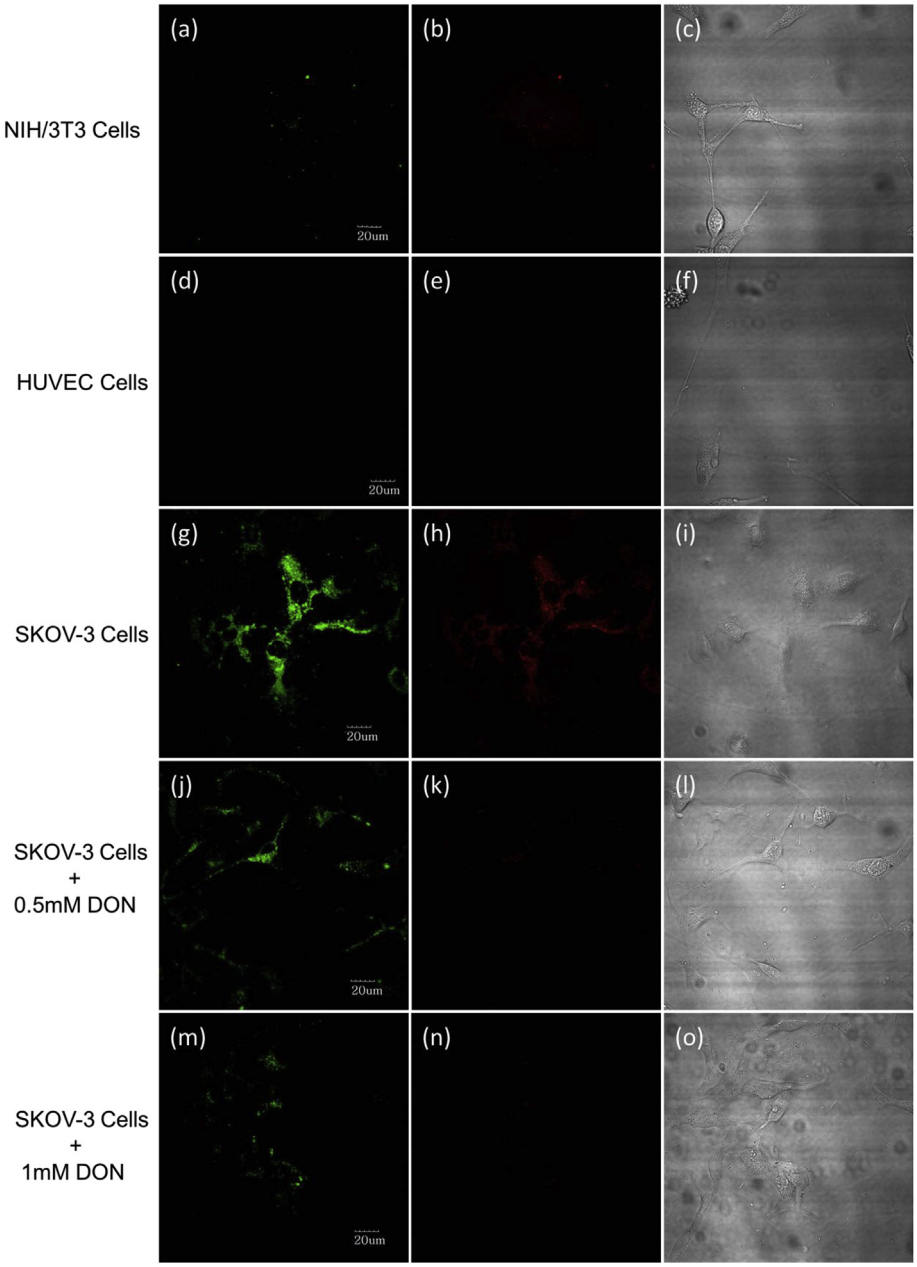

Fig. 3. Fluorescence confocal image of normal cells (NIH/3T3, HUVEC) and cancer cells (SKOV-3) under excitation at 405 nm and emission collected at 490–540 nm for green channel and 570–620 nm for red channel: (a)–(c) NIH/3T3 cells incubated with TAB-3-GSH (10 μM) for 1 h; (d)–(f) HUVEC cells incubated with TAB-3-GSH (10 μM) for 1 h; (g)–(i) SKOV-3 cells incubated with TAB-3-GSH (10 μM) for 1 h; (j)–(o) SKOV-3 cells pretreated with 0.5 mM or 1 mM DON for 1 h and then incubated with TAB-3-GSH (10 μM) for 1 h. (For interpretation of the references to color in this figure legend, the reader is referred to the Web version of this article.)

improved cell membrane permeability of the products than TAB-3-GSH because they bore less carboxyl groups (Fig. S9). Non-cancer human umbilical vein endothelial cells (HUVECs) incubated with TAB-3-GSH for 1 h also presented no fluorescence, while TAB-3-GSH incubated with human ovarian cancer SKOV-3 cells overexpressing GGT, resulted in bright fluorescence under the same experimental conditions (Fig. 3d–i). This can be easily explained from our proposed mechanism, in which GGT can remove the carboxyl groups of TAB-3-GSH by hydrolysis and thus improve the cell membrane permeability of the probe. Thus, our results show that TAB-3-GSH has the ability to differentiate ovarian cancer cells from normal cells. To further confirm that this differentiation potential is due to GGT, we pretreated SKOV-3 cells with a GGT inhibitor, 6-diazo-5-oxo-l-norleucine (DON), and subsequently incubated the cells with TAB-3-GSH. As shown in Fig. 3j–o, the intracellular fluorescence signal decreased significantly when pretreated with 0.5 mM DON and was almost completely absent when pretreated with 1 mM DON. Together, the above experimental results indicate that TAB-3-GSH can be used for selective imaging of cancer cells overexpressing GGT.

Next, we examined the applicability of TAB-3-GSH for targeting tumor in vivo. A nude mouse implanted with subcutaneous xenografts of SKOV-3 cell line at the left posterior axillary was used as the animal model. After intraperitoneal (i.p.) injection of TAB-3-GSH (4 mM, 200 μL), fluorescence signal from the tumors sites were monitored for 1.5 h at every 10min interval. As recorded in Fig. 4, the fluorescence signal appeared in about 60 min and then continually increased for the next 30 min. At 90 min, the tumor area could be clearly located, indicating TAB-3-GSH has the ability for imaging tumor in vivo. As control, another nude mouse with tumor of SKOV-3 at right posterior axillary was pretreated by in-situ injection of DON before the injection

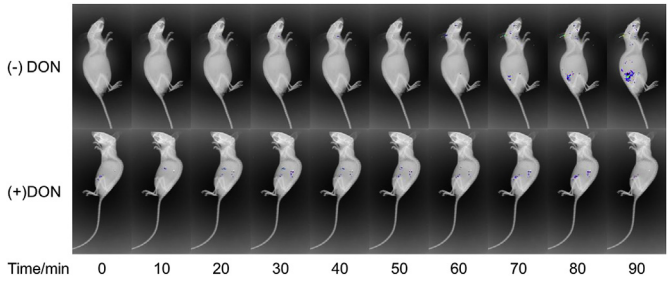

Fig. 4. Time courses of TAB-3-GSH (4 mM, 200 μL) imaging of SKOV-3 tumor (without and with DON pretreatment) in living mice; the fluorescence was monitored at 0, 10, 20, 30, 40, 50, 60, 70, 80, and 90 min.

of TAB-3-GSH. The fluorescence enhancement was obviously inhibited. Thus, TAB-3-GSH could be used effectively to image the GGT-over-expressing SKOV-3 tumor in vivo.

4. Conclusions

A water-soluble fluorescence probe for GGT, TAB-3-GSH, was developed by functionalizing the triarylboron compound with multi GSH groups, which was covalently linked by amide bonds. A series of reference compounds, TAB-3-Cys-Gly, TAB-3-Cys, and TAB-3-GSH-Et, were also synthesized for a comparative study. TAB-3-GSH showed a slight fluorescence response for normal concentration of GGT, but greatly enhanced fluorescence intensity in presence of the abnormal concentration of GGT. Our observations showed that different GGT concentrations can induce hydrolysis reaction at different sites of the molecular structure of TAB-3-GSH: GGT can firstly hydrolyze the amide bond of GSH groups under normal GGT levels and then hydrolyze the amide linkage under abnormally high GGT levels. In cell imaging experiment, TAB-3-GSH could differentiate GGT-overexpressing ovarian cancer cells from normal cells because of its poor cell membrane permeability, which improved after reaction with GGT. Moreover, TAB-3-GSH could also achieve accurate localization to tumor sites in mouse SKOV-3 tumor model. Thus, TAB-3-GSH is a promising probe for targeting GGT-overexpressing tumor in vivo and the proposed mechanism provides a novel strategy for designing fluorescent probes for detecting abnormal concentration of GGT.

Declaration of competing interest

The authors declare that they have no known competing financial interests or personal relationships that could have appeared to influence the work reported in this paper.

CRediT authorship contribution statement

Jun Liu: Investigation, Writing - original draft, Funding acquisition. **Shilu Zhang:** Data curation. **Bin Zhao:** Methodology. **Chengyi Shen:** Writing - review & editing. **Xiaoming Zhang:** Project administration. **Guoqiang Yang:** Writing - review & editing.

Acknowledgement

We are grateful for the funding from the National Natural Science Foundation of China (Grant No. 81801768, 81871440), the Sichuan Science and Technology Department (Grant No. 2019YJ0385), the Scientific Research Project of Sichuan Provincial Department of Education (Grant No. 18ZA0200), the Bureau of Science & Technology and Intellectual Property Nanchong City (Grant No. 16YFZJ0121, 18SXHZ0491) and the North Sichuan Medical College (Grant No. CBY16-QD01).

Appendix A. Supplementary data

Supplementary data to this article can be found online at https://doi.org/10.1016/j.bios.2019.111497.

References

Bae, S.K., Heo, C.H., Choi, D.J., Sen, D., Joe, E.-H., Cho, B.R., Kim, H.M., 2013. J. Am. Chem. Soc. 135, 9915–9923.
Berk, P., Korenblat, K., 2011. In: Goldman, L., Schafer, A.I. (Eds.), Cecil Medicine, 24th edn. Saunders Elsevier, Philadelphia ch. 149.
Blum, G., von Degenfeld, G., Merchant, M.J., Blau, H.M., Bogyo, M., 2007. Nat. Chem. Biol. 3, 668–677.
Bremer, C., Tung, C.-H., Weissleder, R., 2001. Nat. Med. 7, 743–748.
Fraser, A., Ebrahim, S., Smith, G.D., Lawlor, D.A., 2007. Hepatology 46, 158–165.
Gowda, S., Desai, P., Hull, V., Math, A., Venekar, S., Kulkarni, S., 2009. The Pan African Medical Journal 3, 1–11.
Greenlee, R.T., Murray, T., Bolden, S., Wingo, P.A., 2000. Ca-Cancer. J. Clin. 50, 7–33.
Grimm, C., Hofstetter, G., Aust, S., Mutz-Dehbalaie, I., Bruch, M., Heinze, G., Rahhal-Schupp, J., Reinthaller, A., Concin, N., Polterauer, S., 2013. Br. J. Canc. 109, 610–614.
Hanigan, M.H., Frierson, H.F., Brown, J.E., Lovell, M.A., Taylor, P.T., 1994. Cancer Res. 54, 286–290.
Hou, X.F., Yu, Q.X., Zeng, F., Yu, C.M., Wu, S.Z., 2014. Chem. Commun. 50, 3417–3420.
Hu, X., Legler, P.M., Khavrutskii, I., Scorpio, A., Compton, J.R., Robertson, K.L., Friedlander, A.M., Wallqvist, A., 2012. Biochemistry 51, 1199–1212.
Ji, L., Griesbeck, S., Marder, T.B., 2017. Chem. Sci. 8, 846–863.
Jäakle, F., 2010. Chem. Rev. 110, 3985–4022.
Li, X., Guo, X., Cao, L., Xun, Z., Wang, S., Li, S., Li, Y., Yang, G., 2014. Angew. Chem. Int. Ed. 53, 7809–7813.
Li, L.H., Shi, W., Wang, Z., Gong, Q.Y., Ma, H.M., 2015. Anal. Chem. 87, 8353–8359.
Li, S., Hu, R., Yang, C., Zhang, X., Zeng, Y., Wang, S., Guo, X., Li, Y., Cai, X., Li, S., Han, C., Yang, G., 2017a. Biosens. Bioelectron. 325–329.
Li, D.P., Wang, Z.Y., Su, H., Miao, J.Y., Zhao, B.X., 2017b. Chem. Commun. 53, 577–580.
Liu, J., Guo, X., Hu, R., Xu, J., Wang, S., Li, S., Li, Y., Yang, G., 2015. Anal. Chem. 87, 3694–3698.
Liu, J., Guo, X., Hu, R., Liu, X., Wang, S., Li, S., Li, Y., Yang, G., 2016. Anal. Chem. 88, 1052–1057.
Liu, J., Zhang, S., Zhang, C., Dong, J., Shen, C., Zhu, J., Xu, H., Fu, M., Yang, G., Zhang, X., 2017. Chem. Commun. 53, 11476–11479.
Ostapenko, Y.N., Brusin, K.M., Zobnin, Y.V., Shchupak, A.Y., Vishnevetskiy, M.K., Sentsov, V.G., Novikova, O.V., Alekseenko, S.A., Lebed'Ko, O.A., Puchkov, Y.B., 2011. Clin. Toxicol. 49, 471–477.
Ozcan, F., Karakas, M.F., Ozlu, M.F., Akcay, A.B., Buyukkaya, E., Kurt, M., Erden, G., Yuzgecer, H., Yildirimkaya, M., Hajro, E., Balbay, Y., Koc, M., Yazici, H.U., Sen, N., 2012. J. Investig. Med. 60, 1186–1193.
Park, S., Bae, D.J., Ryu, Y.M., Kim, S.Y., Myung, S.J., Kim, H.J., 2016. Chem. Commun. 52, 10400–10402.
Pompella, A., De Tata, V., Paolicchi, A., Zunino, F., 2006. Biochem. Pharmacol. 71, 231–238.
Siegel, R.L., Miller, K.D., Jemal, A., 2018. Ca-Cancer. J. Clin. 68, 7–30.
Tong, H.J., Zheng, Y.J., Zhou, L., Li, X.M., Qian, R., Wang, R., Zhao, J.H., Lou, K.Y., Wang, W., 2016. Anal. Chem. 88, 10816–10820.
Urano, Y., Sakabe, M., Kosaka, N., Ogawa, M., Mitsunaga, M., Asanuma, D., Kamiya, M., Young, M.R., Nagano, T., Choyke, P.L., Kobayashi, H., 2011. Sci. Transl. Med. 3, 110–119.
Vandenhaute, E., Dehouck, L., Boucau, M.C., Sevin, E., Uzbekov, R., Tardivel, M., Gosselet, F., Fenart, L., Cecchelli, R., Dehouck, M.P., 2011. Curr. Neurovascular Res. 8, 258–269.
Wade, C.R., Broomsgrove, A.E.J., Aldridge, S., Gabbai, F.P., 2010. Chem. Rev. 110, 3958–3984.
Wang, F., Zhu, Y., Zhou, L., Pan, L., Cui, Z., Fei, Q., Luo, S., Pan, D., Huang, Q., Wang, R., Zhao, C., Tian, H., Fan, C., 2015. Angew. Chem. Int. Ed. 54, 7349–7353.
Wolfbeis, O.S., 2015. Chem. Soc. Rev. 44, 4743–4768.
Wu, L., Qu, X., 2015. Chem. Soc. Rev. 44, 2963–2997.
Yao, D., Jiang, D., Huang, Z., Lu, J., Tao, Q., Yu, Z., Meng, X., 2000. Cancer 88, 761–769.
Zhou, L., Zhang, X., Wang, Q., Lv, Y., Mao, G., Luo, A., Wu, Y., Wu, Y., Zhang, J., Tan, W., 2014. J. Am. Chem. Soc. 136, 9838–9841.